Polymer Chemistry

ROYAL SOCIETY OF CHEMISTRY

PAPER

View Article Online
View Journal | View Issue

Cite this: *Polym. Chem.*, 2025, **16**, 2840

1,3-Diether-2-methacrylates with glycerol skeletons: tunable resins for stereolithography 3D printing†

Zahra Sekhavat Pour, [a] Pravin S. Shinde, [a] Jun Wang,[a] Cameron Woods,[b] Seth Taylor,[b] Sourav Chatterjee[b] and Jason E. Bara *[a]

Received 26th February 2025,
Accepted 23rd April 2025

DOI: 10.1039/d5py00198f

rsc.li/polymers

The abundance of glycerol associated with biofuel production makes it an interesting substrate for a variety of new molecules. Our prior works have demonstrated the controlled and scalable synthesis of symmetric and asymmetric 1,3-diether-2-propanol compounds with a glycerol skeleton, which serve as versatile intermediates for further chemical modifications. Now we demonstrate that 1,3-diether-2-propanol compounds are useful building blocks to synthesize corresponding methacrylate monomers *via* Steglich esterification with methacrylic anhydride under mild catalytic conditions. The resulting methacrylate monomers were then successfully 3D printed as neat resins using a consumer-level printer. The thermal and mechanical properties of the printed materials were thoroughly investigated. The 3D-printed samples of 1,3-diethoxypropan-2-yl methacrylate (MAA-DEP) possessed good combinations of mechanical and thermal properties, with a tensile strength of 1.61 MPa, elongation at break of 143%, and a glass transition temperature (T_g) near 0 °C. A notable feature of the MAA-DEP monomer is its ability to dissolve polystyrene (PS). Thus, glycerol-based (meth)acrylate monomers present not only new molecules for 3D printing resins with tunable properties but also offer advancements in additive manufacturing by demonstrating how glycerol-derived acrylates also have solvating power to incorporate (waste) thermoplastics into SLA-printable formulations.

1. Introduction

Glycerol, a water-soluble triol, is ubiquitously available and widely utilized across various industries. Among many applications, glycerol serves as a beverage sweetener, an additive in food and cosmetic products, and an antifreeze agent, among other applications. This versatility makes glycerol a valuable compound, yet the increasing production, particularly as a byproduct of the biodiesel industry, has led to a significant surplus. Global biodiesel production is projected to reach 41.4 × 10^9 L by 2025, representing a 33% increase from 2015.[1] This rapid growth is largely driven by efforts to reduce dependence on fossil fuels and promote renewable energy sources. However, for every 100 kg of biodiesel produced, ~10 kg of glycerol is generated as a co-product.[2] Thus, identifying sustainable and innovative applications for excess glycerol is essential to ensure the continued viability of the biodiesel industry. The U.S. Department of Energy (DOE) identifies glycerol as one of the 12 key building block chemicals that can be transformed into various high-value, bio-based chemicals and materials.[3] The three hydroxyl groups on the glycerol molecule provide numerous opportunities for synthesizing a wide range of chemicals with diverse functional groups. The conversion of glycerol into industrial chemicals can be accomplished *via* catalytic pathways, such as oxidation,[4,5] hydrogenation,[6] esterification,[7] transesterification,[8] and etherification.[9,10] These methods open a range of possibilities for transforming glycerol into value-added products for various industrial applications. Moreover, the hydroxyl groups offer the potential to utilize glycerol as a monomer in the synthesis of more sustainable polymeric materials, leading to various valuable applications expanding their industrial and commercial relevance.

In the past decade, significant attention has been devoted to glycerol-based hyperbranched and dendritic polymers, as well as block copolymers, synthesized through condensation polymerization.[11,12] Their biocompatibility and water solubility make them particularly suited for biomedical applications.[13] However, the presence of impurities such as methanol (MeOH) and fatty acid methyl esters (FAMEs) limits the direct use of crude glycerol from the biodiesel industry in biomedical fields (*i.e.*, significant purification is required).[14] As a result, researchers have embarked on searching for novel applications

[a]*Department of Chemical & Biological Engineering, The University of Alabama, Tuscaloosa, AL 35487-0203, USA. E-mail: jbara@eng.ua.edu*
[b]*Department of Chemistry, Murray State University, Murray, KY 42071, USA*
† Electronic supplementary information (ESI) available. See DOI: https://doi.org/10.1039/d5py00198f

of glycerol-based polymers in other industrial sectors. For example, biobased poly(glycerol succinate) was successfully synthesized using crude glycerol and succinic acid to yield an elastomeric bio-polyester.[15] Rigid polyurethane (PU) foams were synthesized by a simple process from a polyol produced by physically mixing castor oil and glycerol in the presence of diisocyanates and a catalyst, presenting great potential to be used in thermal insulation.[16]

The wide range of properties achievable through careful selection of backbone and pendant groups makes (meth)acrylate-based polymers essential in numerous applications, including fabrics, additives, packaging, printing inks, adhesives, construction materials, and automotive paints. This versatility contributes to their substantial global production, which exceeds 9 Mt annually.[17] To shift the (meth)acrylate industry to bio-based materials, one strategy is to develop new bio-based pendant groups offering the same or improved properties compared to conventional, petroleum-derived pendant groups. This transformation would not only support sustainability but also meet the growing demand for eco-friendly materials in these critical industries. Several glycerol derivatives feature acrylate or methacrylate groups, leading to the production of bio-based monomers such as glycerol (meth) acrylate,[18] cyclocarbonate (meth)acrylate,[19] and acetal derivatives such as solketal (meth)acrylate.[14]

We previously demonstrated the controlled synthesis of symmetric and asymmetric 1,3-diether-2-propanol and 1,2,3-alkoxypropane compounds starting from epichlorohydrin (ECH), which is another important molecule that can be derived from glycerol with 2 eq. HCl. While the 1,2,3-trialkoxypropane compounds have clear use as solvents for CO_2 capture,[20,21] the 1,3-diether-2-propanol compounds serve as versatile intermediates to develop other molecules, including esters, ketones, and amines.[10,20,22–24] In this work, we used these 1,3-diether-2-propanol compounds as starting materials to synthesize methacrylate monomers intended to function as key components in 3D printing resins.

The availability and use of 3D printing (*i.e.*, additive manufacturing (AM)) have greatly accelerated in the past decade, enabling the rapid transformation of ideas into physical parts with complex geometries through localized, layer-by-layer material deposition. Among the various 3D printing technologies available – such as inkjet, fused deposition modeling (FDM), digital light processing (DLP), and selective laser sintering (SLS) – stereolithography (SLA) is one of the most established, versatile, and cost-efficient methods. The strategy behind 3D photopolymerization involves the use of liquid-state monomers or oligomers that can be photopolymerized/crosslinked when exposed to a specific wavelength of light in the presence of a photoinitiator.[25] Photopolymerization is often considered a green process due to its high energy efficiency and the potential for solvent-free formulations.[26]

The continuous growth of the resin market for SLA has prompted numerous companies and research groups to develop resins with a wide range of properties.[27,28] Most commercial and multifunctional methacrylate-based monomers such as polyethylene glycol diacrylate (PEGDA),[29] urethane dimethacrylate (UDMA),[30] triethylene glycol dimethacrylate (TEGDMA),[31] and bisphenol A-glycidyl methacrylate (Bis-GMA)[32] are compatible with SLA printers. However, not all resins can meet the requirements for specialized applications, such as self-healing and shape-memory materials, which cannot be achieved using conventional resins. Additionally, sustainable and/or bio-based resins are increasingly favored due to their reduced environmental impact.

In this study, novel UV-curable glycerol-based monomers were developed. The 1,3-diether-2-methacrylates were synthesized through a reaction between symmetric 1,3-diether-2-propanol compounds and methacrylic anhydride (MAA), using a catalyst under mild conditions. These monomers were successfully 3D-printed using a consumer-level SLA printer with an appropriate photoinitiator. Comprehensive studies were systematically conducted to evaluate the thermal and mechanical properties of the 3D-printed objects, highlighting the qualities of these relatively simple monomers to produce objects that are visually indistinguishable from highly formulated commercial resins. Furthermore, the resins have a dual nature as both monomers and solvents, as we have shown that they are able to dissolve relatively high molecular weight polystyrene (PS), which is then incorporated into the 3D printed objects and can be used to tune materials properties.

2. Experimental

2.1. Materials

(±)-ECH (99%) and 2-methoxyethanol (99%) were purchased from Beantown Chemical. ACS grade ethanol (EtOH), methanol (MeOH), dichloromethane (DCM), and sodium hydroxide (NaOH, 97%) were purchased from VWR. Methacrylic anhydride (MAA, 94%) was purchased from Sigma-Aldrich. 4-(Dimethylamino)pyridine (DMAP) was purchased from Chem-Impex int'l. Phenylbis(2,4,6-trimethylbenzoyl)phosphine oxide (BAPO) was purchased from TCI America and used as the initiator. Triethylamine (Et_3N) was purchased from Macron Fine Chemicals. PS was obtained from food containers stamped with resin identification code (RIC) 6. These containers were manually cut into small flakes (0.5–1.0 cm), washed with deionized water and EtOH, and dried at 60 °C in a vacuum oven overnight prior to use.

2.2. Synthesis of symmetric 1,3-diethers

Symmetric 1,3-diether-2-propanol compounds 1,3-dimethoxypropan-2-ol (DMP), 1,3-diethoxypropan-2-ol (DEP), 1,3-dibutoxypropan-2-ol (DBP) and 1,3-bis(2-methoxyethoxy)propan-2-ol (DMEP) were synthesized using methods described in our previous works;[10,22] synthesis of DEP is described briefly in the following section for the convenience of the reader. ^{1}H NMR spectra of the symmetric 1,3-diether-2-propanol compounds were consistent with published results and can be seen in Fig. S1–S4.†

2.2.1. Synthesis of 1,3-diethoxypropan-2-ol (DEP). In a 1000 mL round-bottom flask, EtOH (350 mL, 6.0 mol) and NaOH (56.0 g, 1.4 mol) were heated to 65 °C. After NaOH was completely dissolved, and the mixture cooled to RT, ECH (92.5 g, 1.0 mol) was added dropwise. The reaction was stirred overnight at 65 °C before cooling to RT. The excess EtOH was removed by rotary evaporation under reduced pressure. The mixture was then neutralized with 1 M aq. HCl and the solids were filtered. DEP was further purified by vacuum distillation.

2.3. Synthesis of symmetric 1,3-diether-2-methacrylates

2.3.1. 1,3-Diethoxypropan-2-yl methacrylate (MAA-DEP). The general synthesis of MAA-DEP and other monomers is shown in Fig. 1. The procedure for MAA-DEP is as follows: DEP (20 g, 141 mmol) and 0.1 eq. of DMAP were added to a 250 mL round bottom flask. DCM (60 mL) and Et_3N (1.5 eq.) were added under an Ar atmosphere, followed by the dropwise addition of 1.1 eq. (155 mmol, 23.1 mL) of MAA at room temperature. The final mixture was heated at 45 °C while stirring for 24 h. The solvent was removed under vacuum, and the white solid was filtered. The filtrate was diluted with DCM and washed with saturated $NaHCO_3$ and water several times, before drying over $MgSO_4$. Finally, the solvent was removed *via* rotary evaporation under reduced pressure and dried under vacuum overnight (yield: 23 g, 85%).

Three additional monomers: 1,3-dimethoxypropan-2-yl methacrylate (MAA-DMP), 1,3-dibutoxypropan-2-yl methacrylate (MAA-DBP), and 2,5,9,12-tetraoxatridecan-7-yl methacrylate (MAA-DMEP) were synthesized in the same manner at similar scales from the reaction between corresponding symmetric 1,3-diether-2-propanol compounds and MAA in the presence of Et_3N and DMAP as a catalyst.

2.4. 3D printing of 1,3-diether-2-methacrylates

To prepare resins for SLA 3D printing, the BAPO initiator was added at 2.5 wt% to a certain amount of each monomer and stirred for 10 min until a clear solution was observed. A bottom-up scanning SLA system (Elegoo Mars 4 MSLA, China) with a 405 nm light source was employed for sample fabrication. An exposure time of 40 s was applied to both the base and subsequent layers, with each layer having a thickness of 50 μm. After printing, the unreacted monomer was removed from the surface of the 3D-printed specimens and cleaned with 2-propanol for 10 min. The printed specimens were then post-cured in a UV chamber (Elegoo Mercury Plus) for 10 min.

2.5. Characterization

^1H NMR spectra were collected on a 500 MHz Bruker Avance instrument (Billerica, MA, USA). Viscosities of the four symmetric 1,3-diether-2-methacrylates were measured using a Brookfield DV-II Pro viscometer with a ULA spindle and jacketed sample cell at 25 °C and atmospheric pressure. Temperature control (±0.01 °C) was maintained automatically using a Brookfield TC-602P circulating bath. The density of synthesized monomers was determined using a Mettler Toledo DM45 DeltaRange densitometer at 25 °C and atmospheric pressure. The glass transition temperatures (T_g) of the polymers were determined by differential scanning calorimetry (DSC) (TA Instruments DSC Q20, New Castle, DE, USA) from −40 to 150 °C at a scan rate of 10 °C min^{-1} under a N_2 atmosphere. Heating and cooling cycles were repeated at least three times to ensure reliable and reproducible results. To perform the TGA measurements, an appropriate amount of 3D printed polymer sample was packed in a high-purity cylindrical alumina (Al_2O_3) pan and heated from 25 to 700 °C at a ramp rate of 10 °C min^{-1} under a constant flow rate (10 mL min^{-1}) of ultra-high purity Ar gas (UHP300, Airgas). Tensile testing was conducted utilizing a compact table-top electromechanical-driven single-column load-frame universal testing machine (Test Resources Inc., Shakopee, MN, USA) equipped with a 1.1 kN load cell capacity and a speed range of 0.01 to 30 in min^{-1} controlled by Newton software. The mechanical properties of the specimens were assessed in a controlled environment of 21 ± 2 °C under ASTM D 638 standards 82 mm × 12 mm ×

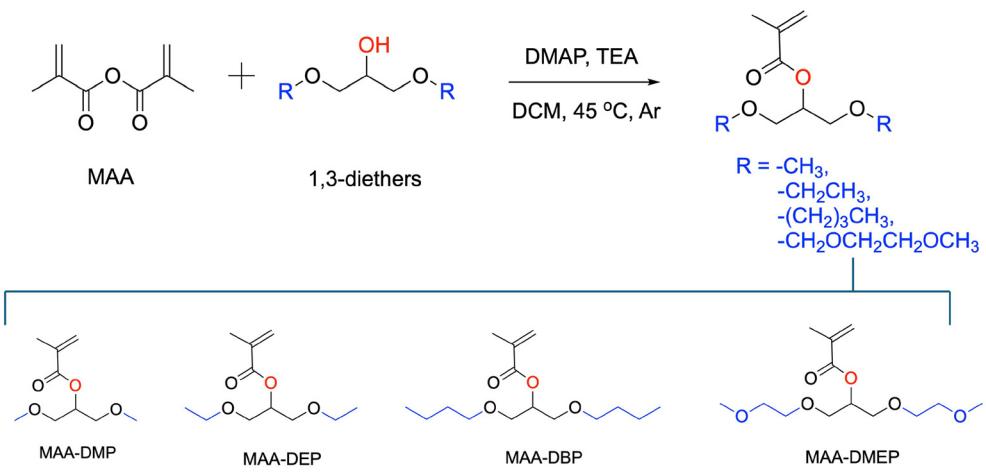

Fig. 1 Synthesis of 1,3-diether methacrylate monomers and their structures.

2 mm. All tensile tests were performed in at least triplicate to ensure reproducibility and statistical reliability.

The degree of C=C double bond conversion (DC, %) in 3D-printed specimens was determined using Fourier transform infrared spectroscopy (FTIR) with a PerkinElmer Spectrum Two ATR-FTIR instrument. This was based on changes in the absorption intensity of the methacrylate C=C stretching vibration at 1638 cm^{-1} before and after photopolymerization. The C=O stretching vibration between 1715 and 1725 cm^{-1} was used as an internal standard. The DC was calculated using the following equation:

$$\mathrm{DC}\,(\%) = \left(1 - \left(\frac{\left(\frac{A_{C=C}}{A_{C=O}}\right)_{\mathrm{Polymer}}}{\left(\frac{A_{C=C}}{A_{C=O}}\right)_{\mathrm{Monomer}}}\right)\right) \times 100$$

where $A_{C=C}$ represents the absorbance at 1638 cm^{-1} before and after photopolymerization, while $A_{C=O}$ refers to the absorbance peak around 1715–1725 cm^{-1} in the monomer and polymer.[33]

SEM images were captured to analyze the morphology of a 3D-printed sample prepared from a 10 wt% solution of PS in MAA-DEP. The samples were cryogenically fractured in liquid N_2, and the fractured surfaces were coated with a thin layer of silver to enhance conductivity. The analysis was conducted using a Thermo Fisher Scientific Apreo 2 SEM instrument operating at 5 kV. XRD measurements were performed on a PANalytical MPD X'pert Pro diffractometer (model: PW3050/60).

3. Results and discussion

3.1. Synthesis method

A series of 1,3-diether-2-methacrylate monomers were synthesized from glycerol-based 1,3-diether-2-propanol compounds and MAA *via* Steglich esterification, using DMAP as the catalyst (Fig. 1). The sole byproduct, methacrylic acid, was easily removed *via* precipitation as a salt with Et_3N. Pure monomers were obtained after washing with aq. $NaHCO_3$ and DI water. Using MAA in Steglich esterification offers several advantages over (meth)acrylic acid, including higher reactivity, eliminating the need for *N*,*N*′-dicyclohexylcarbodiimide (DCC) activation. This results in simpler reaction conditions and complete conversion, avoiding the formation of urea byproducts and reducing the need for extensive purification, such as column chromatography.[34,35] The resulting pure monomers exhibit the ability to dissolve PS, offering a promising strategy for PS upcycling and a significant advancement in additive manufacturing. It is expected that 3D printing of the 1,3-diether-2-methacrylate monomers containing different fractions of PS with different molecular weights will affect the mechanical and thermal properties of the resulting blends. However, this study mainly focuses on the 3D printing of these novel monomers and the characterization of the resulting polymers. More in-depth studies on the effects of PS and other thermoplastics in 1,3-diether-2-methacrylate monomers and their 3D-printed specimens' properties are underway and will be the subject of future studies.

3.2. ^{1}H NMR

The chemical structures of the synthesized 1,3-diether-2-methacrylate monomers were confirmed by ^{1}H NMR spectra, as shown in Fig. S5–S8.† ^{1}H NMR of 1,3-diether-2-propanol starting materials is presented in Fig. S1–S4.† After esterification, new peaks at 6.10, 5.55, and 1.92 ppm were observed, corresponding to the two vinyl protons ($C=CH_2$) and methyl protons (CH_3) of the methacrylate groups, confirming the complete conversion of the hydroxyl groups in the 1,3-diether-2-propanol compounds into methacrylate groups. Additionally, the peak at ~3.7 ppm, attributed to the H on the C atom bound to the hydroxyl group (–CH–OH) in all 1,3-diether-2-propanol compounds, shifted to ~5.2 ppm in the monomer spectra, further demonstrating successful esterification and monomer synthesis.

3.3. Viscosity

The polymerization rate is correlated with its initial viscosity, as viscosity influences the mobility of both monomers and free radicals. This is an important factor in resins used for 3D printing. The structural resolution will be compromised if the resin's viscosity is extremely high or low.[36] Viscosities <3 Pa s (3000 mPa s) at room temperature have effectively produced high-resolution objects using rapid prototyping techniques.[37,38] Table 1 shows the density and viscosity of the synthesized monomers at 25 °C and atmospheric pressure. The density of all samples ranges from ~0.95 g cm^{-3} to 1.01 g cm^{-3}. The viscosity of the monomers increased with the length of the R group chain (see Fig. 1). The MAA-DMP monomer (R: $-CH_3$) exhibited the lowest viscosity at 2.57 mPa s, while the viscosity of MAA-DBP (R: $-(CH_2)_3-CH_3$) more than doubled to 5.53 mPa s. The MAA-DMEP monomer, which has two additional ether groups instead of alkyl chains, exhibited a viscosity close to 5 mPa s. It is important to note that the newly synthesized monomers are not directly comparable to commercial resins in terms of viscosity, as the latter are typically optimized with several additives. Conventional commercial resins usually exhibit viscosities in the range of 200 to 1500 mPa s.[39,40] The 1,3-diether-2-methacrylate monomers can be used as the main component for resin formulation, with viscosity adjusted using crosslinkers and comonomers. Despite the lower viscosity, the printed specimens were suc-

Table 1 Densities (ρ) and viscosities (μ) of 1,3-diether-2-methacrylates at 25 °C and atmospheric pressure

Monomer	ρ (g cm^{-3})	μ (mPa s)
MAA-DMP	1.01106	2.57
MAA-DEP	0.96981	2.80
MAA-DBP	0.94817	5.53
MAA-DMEP	1.05053	4.95
MAA-DEP/PS (10 wt%)	—	166.25

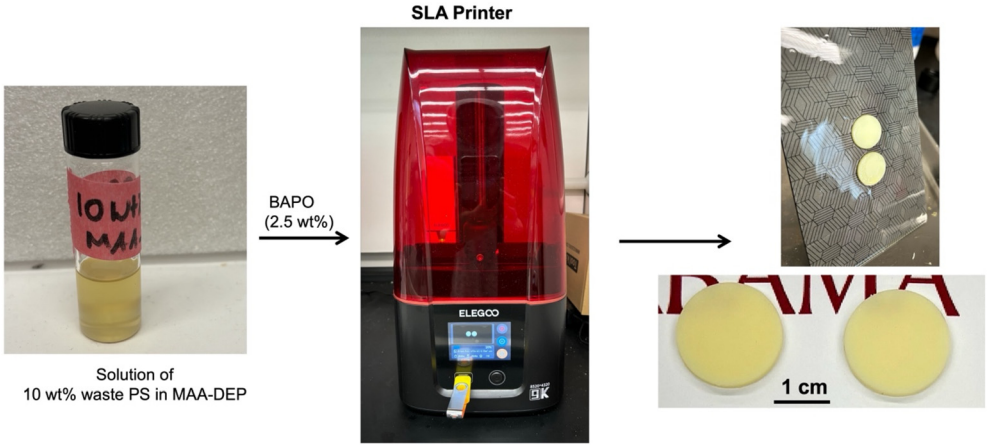

Fig. 2 10 wt% waste PS solution in MAA-DEP and the resulting 3D-printed discs (diameter: 20 mm, thickness: 2 mm).

cessfully fabricated using a consumer-level SLA 3D printer and exhibited well-formed features without major defects. This demonstrates that these resins maintain sufficient resolution for typical layer-based fabrication, even without additional viscosity modifiers.

A special property of 1,3-diether-2-methacrylate monomers, including MAA-DEP, is the ability to dissolve PS (Fig. 2). The viscosity of a 10 wt% waste PS (M_w = 170 kDa) solution in MAA-DEP is also presented in Table 1, showing an increase of ~60× from 2.80 to 166.25 mPa s upon dissolving waste PS with relatively high molecular weight. It was found that PS was soluble in MAA-DEP and other monomers to at least 15 wt% at ambient temperature but the associated increase in viscosity as the PS content increased caused challenges for the printing process.

In all 1,3-diether methacrylate monomers, the C=C double bond of the methacrylate group shows an absorption band at 1638 cm^{-1}, and the ester C=O group exhibits stretching vibrations at 1717–1720 cm^{-1}. The C–H stretching vibrations, characteristic of aliphatic hydrocarbons, appear at around 2950 cm^{-1} and 2865 cm^{-1}, indicating alkyl groups within both the monomers and polymers.[41] A small peak at 3030 cm^{-1} in the MAA-DEP monomer containing 10 wt% PS is attributed to the C–H stretching vibrations of the aromatic ring. After polymerization, all polymer samples exhibited a strong peak at 1723 cm^{-1} (Fig. 3b), corresponding to the C=O stretching vibrations in the methacrylate groups. The C=C absorption at 1638 cm^{-1} in the monomers nearly disappeared, indicating that most of the C=C bonds were polymerized.

The degree of C=C double bond conversion (DC%) was quantified by measuring the reduction in peak absorption intensity at 1638 cm^{-1}, relative to an internal standard (C=O absorption band at 1717–1725 cm^{-1}) that remained unchanged during polymerization. The DC% is a critical parameter for evaluating the photocuring reactivity of resins, and as shown in Table 2, the DC% was ~80% across all resins under the printing conditions used. Nearly all double bonds were polymerized even in the MAA-DEP/PS10 system. This high conversion is likely due to the low viscosity of the 1,3-diether-2-methacrylate monomers, which enhances the mobility of free radicals of the monomers and the growing polymer chains. In contrast, some resins like Bis-GMA, a commonly used monomer in dental composite resins, typically exhibit lower DC values (typically around 55–70%).[32] The high vis-

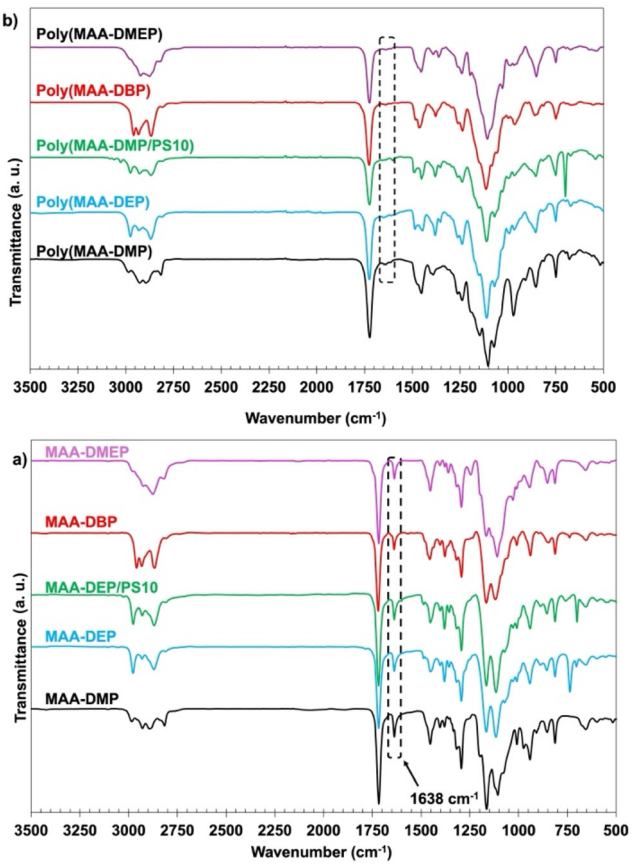

Fig. 3 FTIR spectra of (a) 1,3-diether-2-methacrylate monomers and (b) corresponding polymers.

Table 2 Degree of conversion, thermal properties and average tensile test results of the 3D printed specimens

Polymer	DC (%)	T_g (°C)	$T_{d,max}$[a] (°C)	Young's modulus (MPa)	Tensile strength (MPa)	Elongation at break (%)
Poly(MAA-DMP)	80.2	19.30	320	—	—	—
Poly(MAA-DEP)	78.3	0.29	291	7.67 ± 0.287	1.61 ± 0.097	142.94 ± 7.75
Poly(MAA-DEP)/PS10	80.6	0.72 & 95.82	301	29.83 ± 1.01	3.67 ± 0.159	91.49 ± 6.90
Poly(MAA-DBP)	82.1	27.17	326	8.25 ± 0.279	1.41 ± 0.150	22.87 ± 2.68
Poly(MAA-DMEP)	80.7	26.17	309	2.17 ± 0.087	0.703 ± 0.084	42.90 ± 6.82

[a] Maximum decomposition temperature as measured by TGA.

cosity of Bis-GMA, its rigid bisphenol A (BPA) backbone, and extensive H-bonding restrict polymer chain movement during polymerization, leading to lower conversion rates compared to the more flexible and less viscous 1,3-diether-2-methacrylate monomers synthesized in this work, which share structural commonalities with alkyl methacrylates and poly(ethylene glycol) methacrylates.

3.4. Polymer properties

An SLA 3D printer was utilized to evaluate the suitability of the newly developed 1,3-diether-2-methacrylate monomers for additive manufacturing. BAPO (λ_{max} ~ 370 nm (ref. 26)) was used as the photoinitiator for 3D printing. All monomers were successfully printed and exhibit excellent transparency as shown in Fig. 4a–d. However, the poly(MAA-DMP) printed specimens presented challenges during removal from the build plate, resulting in breakage (Fig. 4a), thus only discs were printed, as opposed to tensile testing dogbones for the other monomers (Fig. 4b–d). To illustrate that the resins were capable of printing parts with fine details, an elephant was printed using poly(MAA-DEP) (Fig. 4e), while Fig. 4f shows that poly(MAA-DEP)/PS10 is translucent.

3.4.1. Thermal properties. The thermal properties of the samples were analyzed using differential scanning calorimetry (DSC) and thermogravimetric analysis (TGA). Fig. 5a and Table 2 present the glass transition temperatures (T_g) of the 3D-printed polymers. The T_g of poly(MAA-DMP) was found to be 19.3 °C, which sharply decreased to 0.29 °C in poly (MAA-DEP). This suggests that adding a single methylene group to each ether moiety significantly increases the flexibility of the polymer chains. In contrast, the longer alkyl side chains in poly(MAA-DBP) and the incorporation of two extra ether groups in the side chain of the MAA-DMEP monomer had the opposite effect, increasing T_g to approximately room temperature. One possible explanation for the increase in T_g with longer alkyl side chains can be attributed to the greater steric hindrance, restricted chain mobility, and chain entanglement imposed by these longer substituents. These longer alkyl groups can increase the polymer's bulkiness, reducing the degree of freedom for the polymer chains' rotation and movement, leading to increased rigidity and a higher T_g. A similar shift toward higher T_g was observed for poly(MAA-DMEP) where the dipole–dipole interactions between extra ether groups might further restrict the movement of the polymer backbone, contributing to the elevated T_g.

The polymer blend produced by the photopolymerization of MAA-DEP with dissolved PS revealed two T_g values (Table 2). The first, at 0.7 °C, corresponds to poly(MAA-DEP), while the second, at 95.8 °C, is attributed to the PS fraction. The presence of two T_g values in the DSC profile of poly(MAA-DEP)/PS10 suggests possible phase separation between the two polymers. The microstructure of this sample will be presented and

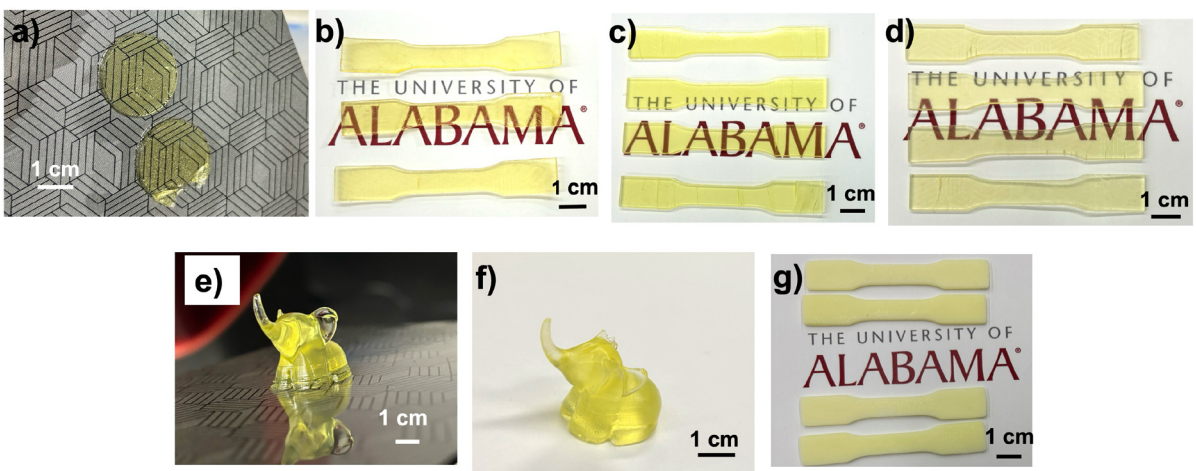

Fig. 4 Photos of 3D printed samples: (a) poly(MAA-DMP) discs on the build plate (diameter: 20 mm, thickness 2 mm), (b) poly(MAA-DEP), (c) poly (MAA-DBP), (d) poly(MAA-DMEP), (e) and (f) 3D printed elephant from MAA-DMEP monomer, and (g) poly(MAA-DEP)/PS10 printed as tensile bars ("dogbones" length: 82 mm, width: 12 mm, and thickness 2 mm).

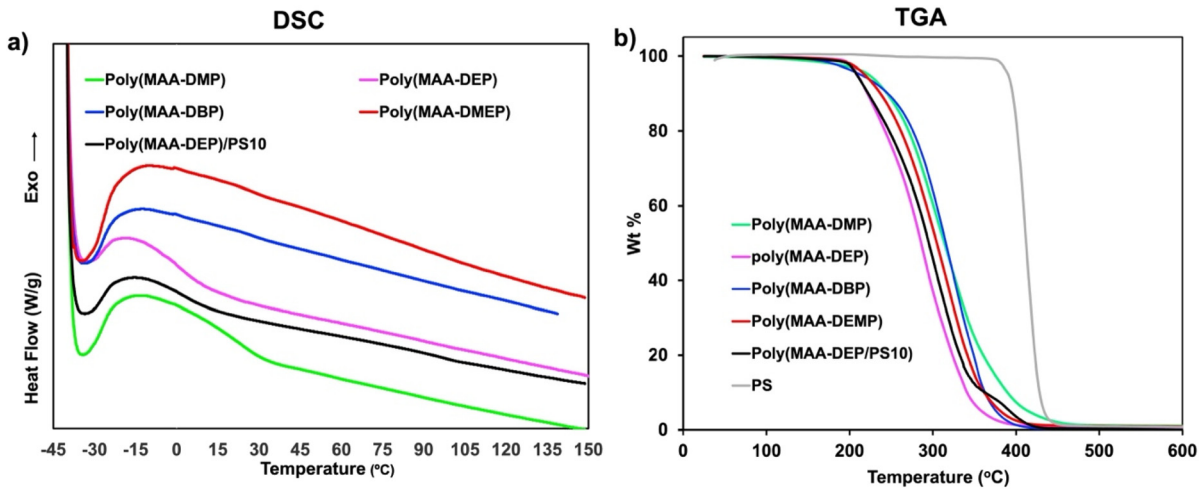

Fig. 5 Thermal properties: (a) DSC and (b) TGA of 3D-printed 1,3-diether methacrylate samples.

discussed in the upcoming section to understand the interaction between the two polymers after 3D printing.

TGA analysis was conducted to assess the thermal stability of the 3D-printed polymer. Fig. 5b shows that the samples exhibit almost similar thermal behavior, with minor variations due to slight structural differences. Thermal decomposition primarily occurs in a single stage. The weight loss below 200 °C was <3% for all samples, with an initial decomposition temperature of around 200 °C. The maximum decomposition temperature ($T_{d,max}$), presented in Table 2, was 326 °C for poly(MAA-DBP) and 291 °C for poly(MAA-DEP), indicating moderate thermal stability. The TGA of poly(MAA-DEP/PS10) shows a distinct but minor decomposition step after the primary decomposition ($T_{d,max}$ = 301 °C), corresponding to a 10 wt% weight loss attributed to PS degradation. However, the $T_{d,max}$ of pure waste PS used is 410 °C; the significant reduction in decomposition temperature within the blend is primarily due to compositional effects that influence the degradation behavior. Specifically, interactions between different species in the blend and their respective degradation products can occur, leading to an accelerated degradation rate and, consequently, a lower $T_{d,max}$ for the PS component within the blend.[42,43]

3.4.2. Microstructural analysis. The microstructures of the cryo-fractured surfaces of pure poly(MAA-DEP) and poly (MAA-DEP) containing 10 wt% dissolved PS are shown in Fig. 6. The samples were fractured in liquid N_2, and the cross-sections were imaged by SEM to assess the morphology and PS domain dispersion in the blend. In Fig. 6a, the fracture surface of pure MAA-DEP exhibits a smooth and homogeneous texture, with no visible evidence of individual printed layers. In contrast, the unique layer-by-layer structure of the 3D-printed sample, with a layer thickness of 50 μm, is clearly observed in the poly(MAA-DEP)/PS blend (Fig. 6b). From Fig. 6c, the PS phase is almost homogeneously dispersed within the main MAA-DEP polymer matrix, with spherical PS domains predominantly concentrated at the top of each layer. It appears that during curing, the poly(MAA-DEP) matrix tends to push the dissolved PS toward the top of each layer. This results in a slightly higher concentration of spherical PS domains with diameters ranging from 0.2 μm to 2 μm at the layer tops. The sponge-like structure observed at the top of each layer, with a thickness of approximately 10 μm, may be attributed to this phenomenon. Additionally, these phase boundaries scatter light, leading to reduced transparency and causing the material to appear translucent/opaque (Fig. 2).[44]

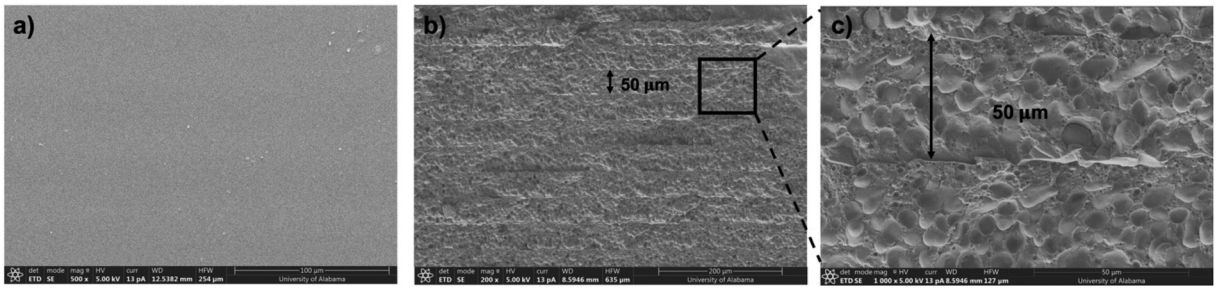

Fig. 6 SEM images of cryo-fractured cross-sections of 3D-printed samples prepared from tensile bars: (a) poly(MAA-DEP) and (b and c) poly (MAA-DEP)/PS (10 wt%).

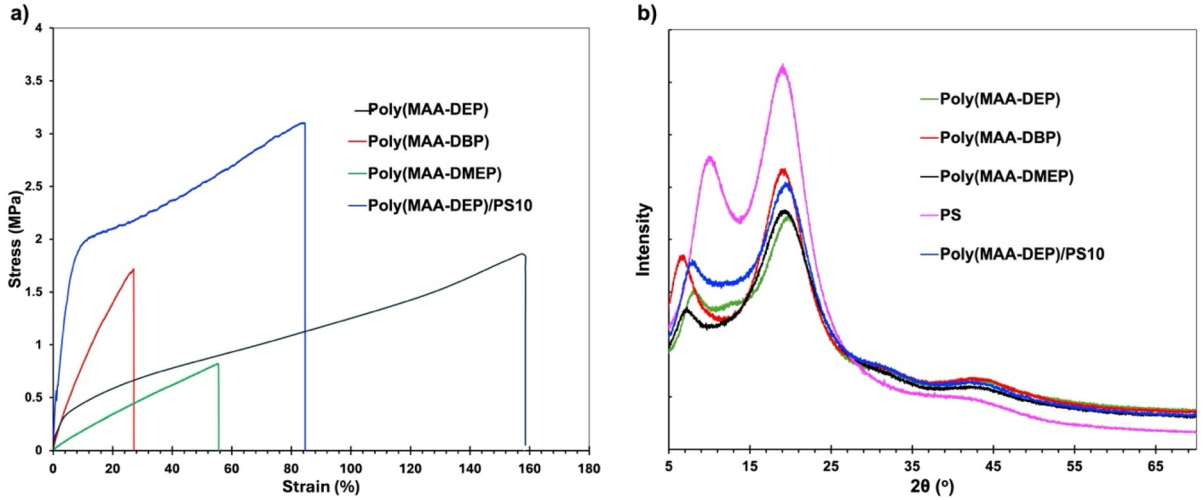

Fig. 7 (a) Stress–strain curves and (b) XRD patterns of 3D-printed 1,3-diether-2-methacrylate polymers.

This morphology is expected to influence the mechanical properties of the resulting 3D-printed blend. While polymer blends are typically synthesized through melt blending in equipment such as extruders, the dual functions of MAA-DEP as both a monomer and a solvent provide an innovative approach to preparing polymer blends through a fundamentally different method.

3.4.3. Mechanical properties. Tensile tests were conducted on the 3D-printed dogbone specimens to evaluate the effects of the chemical structure of 1,3-diether-2-methacrylates on the mechanical properties of the resultant polymers. The average tensile strength (MPa), Young's modulus (MPa), and elongation at break (%) are summarized in Table 2, and the stress–strain curves are shown in Fig. 7a. Poly(MAA-DEP) and poly (MAA-DBP) exhibit similar Young's modulus values of 7.67 and 8.25 MPa, respectively, indicating that they are stiffer than poly(MAA-DMEP), which has a Young's modulus of 2.17 MPa. The maximum tensile strength of 1.61 was observed for poly (MAA-DEP), which is more than twice that of poly(MAA-DMEP) (0.70 MPa). In terms of elongation at break, poly(MAA-DEP) also demonstrated a superior strain of approximately 143%, which is more than 6× that of poly(MAA-DMEP). These results show that the mechanical properties of these 3D-printed polymers depend significantly on the chemical structure of the 1,3-diether-2-methacrylate monomers. Poly(MAA-DEP) demonstrates the best mechanical performance within the series, indicating that its chemical structure is optimal for achieving 3D-printed items with mechanical properties comparable to some thermoplastic polyurethane (TPU)[45–47] and poly(ether-*block*-amide)[48,49] materials. These properties make it suitable for applications demanding flexibility and elasticity, such as footwear, sporting goods, medical devices, and seals. The strength and performance of the resulting polymers can be customized by formulating a resin with different crosslinkers, co-monomers, and filler-filling reinforcement. Dissolving waste PS at 10 wt% in MAA-DEP significantly enhances the tensile properties of the 3D-printed polymer (Fig. 7a). The tensile strength more than doubles compared to that of poly (MAA-DEP), and the Young's modulus increases approximately 4×, reaching ~30 MPa. This increase is attributed to the inherent high tensile strength and modulus of PS. The reduction in elongation at break to nearly 90% is due to the formation of rigid PS domains (Fig. 6) during the photopolymerization of MAA-DEP, which restricts the overall flexibility of the material, making it stiffer and less stretchable.

3.4.4. XRD studies. XRD is a non-destructive technique used to analyze the morphology of polymers and their blends. Fig. 7b presents the diffractograms of 3D-printed 1,3-diether-2-methacrylate polymers within the 2θ range of 5° to 70°. The XRD spectra of all 3D-printed 1,3-diether-2-methacrylate polymers exhibit a predominantly amorphous nature, characterized by the absence of sharp, distinct diffraction peaks. For example, the diffractogram of poly(MAA-DEP) exhibits four broad peaks at 2θ values of 8.01°, 19.76°, 32.74°, and 43.97°, with a gradual decrease in peak intensity. Variations in the pendant groups of the monomers do not induce crystallinity in the resulting polymers and do not have a significant effect on the peak positions.

Neat PS exhibits two distinct broad peaks at 9.89° and 19.10°, confirming its amorphous character. Incorporating 10 wt% PS into MAA-DEP, followed by 3D printing, resulted in a blend without altering the peak positions in the XRD spectra. This consistency further supports the uniform distribution of the PS in the blend.[50]

4. Conclusion

Developing 3D printing resins from renewable and/or waste feedstocks represents an opportunity toward a more sustainable polymer industry. In this work, functional methacrylate monomers based on glycerol skeletons were synthesized from

1,3-diether-2-propanol compounds with MAA under mild catalytic conditions. The resulting 1,3-diether-2-methacrylate monomers, which were of relatively low viscosity, were successfully used for SLA 3D printing in the presence of a UV initiator, achieving high C=C double bond conversion. Among the series of 3D-printed polymers obtained, poly(MAA-DEP) exhibited the best combination of mechanical and thermal properties, including the lowest glass transition temperature (approximately 0 °C), and the highest tensile strength and elongation at break. The ability of MAA-DEP to dissolve high molecular weight PS is particularly promising, as it not only offers opportunities to tailor polymer properties but also facilitates PS upcycling. These findings provide valuable insights for enhancing the properties and performances of 3D printing resins and contributing to the development of sustainable materials.

Data availability

The data supporting this article have been included as part of the ESI.†

Conflicts of interest

There are no conflicts to declare.

Acknowledgements

The authors gratefully acknowledge support from the U.S. National Science Foundation (EFMA-2029387). The images within the TOC graphic were created by the authors using AI generative software (Adobe Firefly). The authors' university has a license for Adobe Firefly and the terms of use associated with the software are being followed. All other images/photographs were fully created by the authors.

References

1 H. I. Mahdi, N. N. Ramlee, J. L. da Silva Duarte, Y.-S. Cheng, R. Selvasembian, F. Amir, L. H. de Oliveira, N. I. W. Azelee, L. Meili and G. Rangasamy, A comprehensive review on nanocatalysts and nanobiocatalysts for biodiesel production in Indonesia, Malaysia, Brazil and USA, *Chemosphere*, 2023, **319**, 138003.
2 S. Goyal, N. B. Hernández and E. W. Cochran, An update on the future prospects of glycerol polymers, *Polym. Int.*, 2021, **70**(7), 911–917.
3 T. A. Werpy, J. E. Holladay and J. F. White, *Top value added chemicals from biomass: I. Results of screening for potential candidates from sugars and synthesis gas*, Pacific Northwest National Lab.(PNNL), Richland, WA (United States), 2004.
4 A. Villa, N. Dimitratos, C. E. Chan-Thaw, C. Hammond, L. Prati and G. J. Hutchings, Glycerol oxidation using gold-containing catalysts, *Acc. Chem. Res.*, 2015, **48**(5), 1403–1412.
5 M. K. Goetz, M. T. Bender and K.-S. Choi, Predictive control of selective secondary alcohol oxidation of glycerol on NiOOH, *Nat. Commun.*, 2022, **13**(1), 5848.
6 R. H. Crabtree, *Transfer hydrogenation with glycerol as H-donor: Catalyst activation, deactivation and homogeneity*, ACS Publications, 2019.
7 R. Mou, X. Wang, Z. Wang, D. Zhang, Z. Yin, Y. Lv and Z. Wei, Synthesis of fuel bioadditive by esterification of glycerol with acetic acid over hydrophobic polymer-based solid acid, *Fuel*, 2021, **302**, 121175.
8 A. Das, D. Shi, G. Halder and S. L. Rokhum, Microwave-assisted synthesis of glycerol carbonate by transesterification of glycerol using Mangifera indica peel calcined ash as catalyst, *Fuel*, 2022, **330**, 125511.
9 P. Palanychamy, S. Lim, Y. H. Yap and L. K. Leong, Critical review of the various reaction mechanisms for glycerol etherification, *Catalysts*, 2022, **12**(11), 1487.
10 S. Qian, X. Liu, V. N. Emel'yanenko, P. Sikorski, I. Kammakakam, B. S. Flowers, T. A. Jones, C. H. Turner, S. P. Verevkin and J. E. Bara, Synthesis and properties of 1, 2, 3-Triethoxypropane: a glycerol-derived green solvent candidate, *Ind. Eng. Chem. Res.*, 2020, **59**(45), 20190–20200.
11 M. A. Carnahan and M. W. Grinstaff, Synthesis and characterization of poly (glycerol– succinic acid) dendrimers, *Macromolecules*, 2001, **34**(22), 7648–7655.
12 V. T. Wyatt, Lewis acid-catalyzed synthesis of hyperbranched polymers based on glycerol and diacids in toluene. *Journal of the American Oil Chemists'*, *Society*, 2012, **89**, 313–319.
13 H. Zhang and M. W. Grinstaff, Synthesis of atactic and isotactic poly (1, 2-glycerol carbonate) s: degradable polymers for biomedical and pharmaceutical applications, *J. Am. Chem. Soc.*, 2013, **135**(18), 6806–6809.
14 S. Goyal, F.-Y. Lin, M. Forrester, W. Henrichsen, G. Murphy, L. Shen, T.-P. Wang and E. W. Cochran, Glycerol ketals as building blocks for a new class of biobased (meth) acrylate polymers, *ACS Sustainable Chem. Eng.*, 2021, **9**(31), 10620–10629.
15 O. Valerio, T. Horvath, C. Pond, M. Misra and A. Mohanty, Improved utilization of crude glycerol from biodiesel industries: Synthesis and characterization of sustainable biobased polyesters, *Ind. Crops Prod.*, 2015, **78**, 141–147.
16 C. S. Carriço, T. Fraga, V. E. Carvalho and V. M. Pasa, Polyurethane foams for thermal insulation uses produced from castor oil and crude glycerol biopolyols, *Molecules*, 2017, **22**(7), 1091.
17 I. Gaytán, M. Burelo and H. Loza-Tavera, Current status on the biodegradability of acrylic polymers: microorganisms, enzymes and metabolic pathways involved, *Appl. Microbiol. Biotechnol.*, 2021, **105**, 991–1006.
18 M. Forrester, A. Becker, A. Hohmann, N. Hernandez, F.-Y. Lin, N. Bloome, G. Johnson, H. Dietrich, J. Marcinko and R. C. Williams, RAFT thermoplastics from glycerol: a

biopolymer for development of sustainable wood adhesives, *Green Chem.*, 2020, **22**(18), 6148–6156.
19 A. Zanoni, G. Gardoni, M. Sponchioni and D. Moscatelli, Valorisation of glycerol and CO2 to produce biodegradable polymer nanoparticles with a high percentage of bio-based components, *J. CO2 Util.*, 2020, **40**, 101192.
20 S. Qian, X. Liu, C. H. Turner and J. E. Bara, Synthesis and properties of symmetric glycerol-derived 1, 2, 3-triethers and 1, 3-diether-2-ketones for CO2 absorption, *Chem. Eng. Sci.*, 2022, **248**, 117150.
21 I. V. Andreeva, V. V. Turovtsev, S. Qian, J. E. Bara and S. P. Verevkin, Biofuel Additives: Thermodynamic Studies of Glycerol Ethers, *Ind. Eng. Chem. Res.*, 2022, **61**(41), 15407–15413.
22 S. Qian, X. Liu, G. P. Dennis, C. H. Turner and J. E. Bara, Properties of symmetric 1, 3-diethers based on glycerol skeletons for CO2 absorption, *Fluid Phase Equilib.*, 2020, **521**, 112718.
23 S. Qian, J. D. Leah, S. Chatterjee, A. Soyemi, T. Szilvási and J. E. Bara, Properties of Imidazolium Ionic Liquids with Glycerol-Derived Functional Groups, *J. Chem. Eng. Data*, 2022, **67**(8), 1905–1914.
24 S. Chatterjee, S. Qian, A. Soyemi, T. Szilvási and J. E. Bara, Synthesis and Properties of 2-Halo-1, 3-diether-propanes: Diversifying the Range of Functionality in Glycerol-Derived Compounds, *Ind. Eng. Chem. Res.*, 2023, **62**(6), 2959–2967.
25 A. Bagheri and J. Jin, Photopolymerization in 3D printing, *ACS Appl. Polym. Mater.*, 2019, **1**(4), 593–611.
26 J. Zhang and P. Xiao, 3D printing of photopolymers, *Polym. Chem.*, 2018, **9**(13), 1530–1540.
27 G. Scordo, V. Bertana, L. Scaltrito, S. Ferrero, M. Cocuzza, S. L. Marasso, S. Romano, R. Sesana, F. Catania and C. F. Pirri, A novel highly electrically conductive composite resin for stereolithography, *Mater. Today Commun.*, 2019, **19**, 12–17.
28 L. Zhou, W. Ning, C. Wu, D. Zhang, W. Wei, J. Ma, C. Li and L. Chen, 3D–printed microelectrodes with a developed conductive network and hierarchical pores toward high areal capacity for microbatteries, *Adv. Mater. Technol.*, 2019, **4**(2), 1800402.
29 M. Hakim Khalili, V. Panchal, A. Dulebo, S. Hawi, R. Zhang, S. Wilson, E. Dossi, S. Goel, S. A. Impey and A. I. Aria, Mechanical Behavior of 3D Printed Poly (ethylene glycol) Diacrylate Hydrogels in Hydrated Conditions Investigated Using Atomic Force Microscopy, *ACS Appl. Polym. Mater.*, 2023, **5**(4), 3034–3042.
30 A. A. Abu Bakar, M. Z. Zainuddin, S. M. Abdullah, N. Tamchek, I. S. Mohd Noor, M. S. Alauddin, A. Alforidi and M. I. Mohd Ghazali, The 3D printability and mechanical properties of polyhydroxybutyrate (PHB) as additives in urethane dimethacrylate (UDMA) blends polymer for medical application, *Polymers*, 2022, **14**(21), 4518.
31 P. Comeau and T. Willett, Triethyleneglycol dimethacrylate addition improves the 3D-printability and construct properties of a GelMA-nHA composite system towards tissue engineering applications, *Mater. Sci. Eng., C*, 2020, **112**, 110937.
32 Y. Choi, J. Yoon, J. Kim, C. Lee, J. Oh and N. Cho, Development of bisphenol-A-glycidyl-methacrylate-and trimethylolpropane-triacrylate-based Stereolithography 3D printing materials, *Polymers*, 2022, **14**(23), 5198.
33 J.-J. Tzeng, T.-S. Yang, W.-F. Lee, H. Chen and H.-M. Chang, Mechanical properties and biocompatibility of urethane acrylate-based 3D-printed denture base resin, *Polymers*, 2021, **13**(5), 822.
34 F. J. S. Xavier, K. A. D. F. Rodrigues, R. G. De Oliveira, C. G. Lima Junior, J. D. C. Rocha, T. S. L. Keesen, M. R. De Oliveira, F. P. L. Silva and M. L. A. D. A. Vasconcellos, Synthesis and in vitro anti Leishmania amazonensis biological screening of Morita-Baylis-Hillman adducts prepared from eugenol, thymol and carvacrol, *Molecules*, 2016, **21**(11), 1483.
35 C. Bonneaud, M. Decostanzi, J. Burgess, G. Trusiano, T. Burgess, R. Bongiovanni, C. Joly-Duhamel and C. M. Friesen, Synthesis of α, β-unsaturated esters of perfluoropolyalkylethers (PFPAEs) based on hexafluoropropylene oxide units for photopolymerization, *RSC Adv.*, 2018, **8**(57), 32664–32671.
36 T. D. Ngo, A. Kashani, G. Imbalzano, K. T. Nguyen and D. Hui, Additive manufacturing (3D printing): A review of materials, methods, applications and challenges, *Composites, Part B*, 2018, **143**, 172–196.
37 Z. Weng, Y. Zhou, W. Lin, T. Senthil and L. Wu, Structure-property relationship of nano enhanced stereolithography resin for desktop SLA 3D printer, *Composites, Part A*, 2016, **88**, 234–242.
38 M. Wozniak, Y. de Hazan, T. Graule and D. Kata, Rheology of UV curable colloidal silica dispersions for rapid prototyping applications, *J. Eur. Ceram. Soc.*, 2011, **31**(13), 2221–2229.
39 S. Grauzeliene, M. Kastanauskas, V. Talacka and J. Ostrauskaite, Photocurable glycerol-and Vanillin-based resins for the synthesis of vitrimers, *ACS Appl. Polym. Mater.*, 2022, **4**(8), 6103–6110.
40 R. J. Pugh and L. Bergstrom, *Surface and colloid chemistry in advanced ceramics processing*, CRC Press, 1993.
41 S. Ganesamoorthy, H. Prabhakaran, S. O. Kanemoto, A. M. Y. Cheumani and M. S. Lakshmi, Titanium nanoparticles bonded polyacrylates with enhanced properties fabricated using dlp 3D printing, *J. Polym. Res.*, 2024, **31**(1), 21.
42 F. P. La Mantia, M. Morreale, L. Botta, M. C. Mistretta, M. Ceraulo and R. Scaffaro, Degradation of polymer blends: A brief review, *Polym. Degrad. Stab.*, 2017, **145**, 79–92.
43 N. Netsch, L. Schröder, M. Zeller, I. Neugber, D. Merz, C. O. Klein, S. Tavakkol and D. Stapf, Thermogravimetric study on thermal degradation kinetics and polymer interactions in mixed thermoplastics, *J. Therm. Anal. Calorim.*, 2025, **150**(1), 211–229.
44 T. Bubmann, A. Seidel and V. Altstädt, Transparent PC/PMMA blends via reactive compatibilization in a twin-screw extruder, *Polymers*, 2019, **11**(12), 2070.
45 H. Lee, R.-I. Eom and Y. Lee, Evaluation of the mechanical properties of porous thermoplastic polyurethane obtained

by 3D printing for protective gear, *Adv. Mater. Sci. Eng.*, 2019, **2019**(1), 5838361.
46 C. Ge, Q. Ren, S. Wang, W. Zheng, W. Zhai and C. B. Park, Steam-chest molding of expanded thermoplastic polyurethane bead foams and their mechanical properties, *Chem. Eng. Sci.*, 2017, **174**, 337–346.
47 A. F. Osman, G. A. Edwards, T. L. Schiller, Y. Andriani, K. S. Jack, I. C. Morrow, P. J. Halley and D. J. Martin, Structure–property relationships in biomedical thermoplastic polyurethane nanocomposites, *Macromolecules*, 2012, **45**(1), 198–210.
48 Z. Xu, G. Wang, J. Zhao, A. Zhang and G. Zhao, Superelastic and structure-tunable poly (ether-block-amide) foams achieved by microcellular foaming, *J. CO2 Util.*, 2022, **55**, 101807.
49 Y. Shibasaki, R. Kudo, T. Tsukamoto and Y. Oishi, Synthesis of thermosetting poly (amide-ether) block copolymers and their shape memory properties, *React. Funct. Polym.*, 2022, **176**, 105293.
50 S. Ahmad, S. Ahmad and S. Agnihotry, Synthesis and characterization of in situ prepared poly (methyl methacrylate) nanocomposites, *Bull. Mater. Sci.*, 2007, **30**, 31–35.